Earth and Planetary Science Letters 388 (2014) 134–142

Contents lists available at ScienceDirect

Earth and Planetary Science Letters

www.elsevier.com/locate/epsl

Dynamic recrystallization and phase mixing in experimentally deformed peridotite

Jolien Linckens, Rolf H.C. Bruijn *, Philip Skemer

Washington University in St. Louis, Earth and Planetary Sciences, One-Brookings Drive, Campus Box 1169, Saint Louis, MO 63130, United States

ARTICLE INFO

Article history:
Received 28 June 2013
Received in revised form 9 November 2013
Accepted 16 November 2013
Available online xxxx
Editor: Y. Ricard

Keywords:
dynamic recrystallization
phase mixing
grain boundary sliding
shear localization
piezometer
peridotite

ABSTRACT

Ductile shear zones evolve through complex feedbacks between microstructure and rheology. In the mantle, shear zones often display mylonitic or ultramylonitic microstructures, characterized by extensive grain-size reduction and well-mixed polymineralic domains. The feedback between the formation of these microstructures and grain-size sensitive deformation is often considered an important weakening mechanism in high-temperature mantle shear zones. To understand better the processes that transform coarse-grained tectonites into fine-grained and well-mixed mylonites, we have performed triaxial deformation experiments on synthetic peridotite samples comprised of mm-scale olivine and orthopyroxene clasts. Experiments were conducted in a Griggs apparatus at a confining pressure of ~1 GPa, temperatures of 1400 to 1550 K and strain rates of 10^{-5}–10^{-6} s^{-1} under nominally dry conditions. Experiments yield deformed samples with macroscopic natural strains ranging from 0.31 to 0.74. Samples are partially recrystallized, with neoblasts ranging in grain size from 2–25 μm. At these deformation conditions, unrecrystallized mm-sized clasts deform by grain-size insensitive dislocation creep, while recrystallized grains deform by grain-size sensitive dislocation accommodated grain boundary sliding (disGBS). Using electron-backscatter diffraction (EBSD) we investigate the interfaces between recrystallized olivine and orthopyroxene domains. At the majority of these interfaces no mixing is observed. However, many boundaries are serrated, which is interpreted to be the result of surface tension driven phase boundary migration. In a few cases we observe small degrees of mixing, with enclaves of one phase completely surrounded by the other phase. This mixing occurs only within a few recrystallized grain length scales of the interface. These results demonstrate that the serial processes of dynamic recrystallization, phase boundary migration and disGBS deformation are a plausible mechanism for solid-state phase mixing. However, more extensive deformation may be needed to reproduce the near steady-state microstructure observed in highly deformed mantle shear zones.

1. Introduction

The strength and dynamics of the lithosphere, the initiation of subduction, and the generation of Earth-like plate tectonics are all strongly influenced by the ability of the lithosphere to localize deformation (e.g. Bercovici, 2003; Bercovici and Ricard, 2012, 2013; Bürgmann and Dresen, 2008; Carter and Tsenn, 1987; Kirby, 1985; Précigout et al., 2007; Regenauer-Lieb et al., 2001; Tommasi et al., 2009; Vauchez et al., 2012; Vissers et al., 1995; Warren and Hirth, 2006). High temperature ductile shear zones, which are considered manifestations of shear localization, are typically characterized by grain sizes that are significantly smaller than the grain size in the associated host rock (Drury et al., 1991; White et al., 1980). The smaller grain size is generally interpreted to be the product of dynamic recrystallization, as mechanical work associated with deformation is converted to additional grain boundary area (e.g. Austin and Evans, 2007; Rozel et al., 2011). Grain-size reduction is also often associated with an inferred transition in deformation mechanism, from dislocation creep to diffusion creep or dislocation accommodated grain boundary sliding (disGBS) (Dijkstra et al., 2002; Handy, 1989; Jaroslow et al., 1996; Jin et al., 1998; Linckens et al., 2011; Newman et al., 1999; Précigout et al., 2007; Skemer et al., 2010; Toy et al., 2010; Vissers et al., 1995; Warren and Hirth, 2006).[1]

The activation of grain size sensitive deformation mechanisms is expected to promote rheological weakening (Hansen et al., 2011; Hirth and Kohlstedt, 2003; Rutter and Brodie, 1988; Walker et al., 1990). However, weakening caused by a reduction in grain

* Corresponding author. Tel.: +1 314 935 6652.
E-mail addresses: jlinckens@levee.wustl.edu (J. Linckens), bruijn@levee.wustl.edu (R.H.C. Bruijn), pskemer@wustl.edu (P. Skemer).

0012-821X/$ – see front matter
http://dx.doi.org/10.1016/j.epsl.2013.11.037

[1] In the present study, we use the term disGBS to denote the phenomenon observed experimentally in olivine by Hirth and Kohlstedt (2003) and Hansen et al. (2011) at conditions intermediate between dislocation creep and diffusion creep.

size is countered by the tendency of grains to coarsen with time (De Bresser et al., 1998). When grain growth kinetics are rapid in comparison to dynamic recrystallization, as is the case for olivine (Karato, 1989), a material's ability to localize deformation is strongly inhibited. However, it is well known that secondary phases inhibit grain growth (Evans et al., 2001; Olgaard and Evans, 1986; Smith, 1948) and the inhibition of grain growth by well-mixed primary and secondary phases may therefore facilitate long-lived weakening in polymineralic shear zones (Farla et al., 2013; Herwegh et al., 2011; Linckens et al., 2011; Michibayashi et al., 2013; Précigout et al., 2007). Indeed, intermixed olivine and pyroxene are commonly observed in peridotite mylonites and ultramylonites (Dijkstra et al., 2002; Linckens et al., 2011; Newman et al., 1999; Skemer et al., 2010; Toy et al., 2010; Warren and Hirth, 2006). However, the processes that lead to phase mixing are not readily inferred from the geologic record. Some authors have speculated that grain boundary sliding (cf. Ashby and Verrall, 1973) may promote phase mixing (Linckens et al., 2011; Warren and Hirth, 2006). Others have argued that mixing occurs through particular metamorphic or melt-rock reactions (Dijkstra et al., 2002; Furusho and Kanagawa, 1999; Kelemen and Dick, 1995; Newman et al., 1999) or by entrainment of adjacent materials (Toy et al., 2010). Recent experimental studies designed to evaluate the development or preservation of phase mixing in fine-grained olivine–pyroxene aggregates show conflicting results: Hiraga et al. (2013) interpret their results as evidence of phase coalescence with progressive strain, while Farla et al. (2013) interpret their results as evidence of phase mixing.

To improve our understanding of phase mixing and the conditions at which it occurs, we performed high pressure, high temperature deformation experiments on synthetic peridotite samples, consisting of coarse-grained (mm-size) olivine and orthopyroxene clasts, embedded in a fine-grained (<10 μm) olivine matrix (Fig. 1). Previous deformation experiments on synthetic olivine–orthopyroxene aggregates started with fine-grained, well-mixed olivine and pyroxene powders (Farla et al., 2013; Hiraga et al., 2010, 2013; Hitchings et al., 1989; Ji et al., 2001; Lawlis, 1998; McDonnell et al., 2000; Sundberg and Cooper, 2008). Due to the small grain size and homogeneity of the starting materials in these studies, recrystallization and phase mixing or phase coalescence are difficult to identify on the basis of microstructure alone. In contrast, the starting materials in our experiments are coarse-grained, with mineral domain length scales that are initially two-three orders of magnitude larger than the recrystallized grain-size. This experimental design has a number of benefits. First, we are able to compare recrystallization processes in olivine and orthopyroxene directly with no complexity introduced by the mutual pinning of the two phases. Second, we are able to make unambiguous observations of the mixing process along initially unmixed mineral domain interfaces.

Our results demonstrate that the processes leading to a well-mixed microstructure are inefficient at the conditions achieved in these experiments. The serial processes of grain-size reduction by dynamic recrystallization, phase mixing, and subsequent deformation by disGBS likely contribute to the long-lived weakness of ductile shear zones, but may not play a major role in the initiation of shear localization.

2. Methods

Triaxial deformation experiments were conducted in a Griggs apparatus at a confining pressure of ~1 GPa, temperatures of 1400 to 1550 K and strain-rates of 10^{-5}–10^{-6} s^{-1} (Table 1). The experimental charges consisted of large (~0.5–2 mm) sub-spherical clasts of olivine and orthopyroxene embedded in fine-grained (<10 μm) matrix of olivine powder (Fig. 1). Starting materials were synthesized from one to three mm diameter, inclusion-free olivine (Fo_{90}) and orthopyroxene fragments hand-picked from xenoliths of San Carlos peridotite. Smooth-surfaced sub-spherical clasts of both olivine and orthopyroxene were produced by running the rough fragments through a fluid energy mill and selecting clasts with an aspect ratio (i.e. longest axis over shortest axis) smaller than 1.5.

Table 1
Experimental parameters. The confining pressure for all experiments is ~1 GPa.

Experiment	Temperature (K)	Strain rate ($\times 10^{-5}$ s^{-1})	Natural strain[1]
WUG_64	1400	3.9	0.48
WUG_67	1400	4.0	0.43
WUG_69	1450	4.0	0.54
WUG_73	1450	4.0	0.58
WUG_18	1500	4.4	0.52
WUG_113	1500	0.6	0.74
WUG_115	1500	0.7	0.64
WUG_76	1500	3.9	0.45
WUG_119	1525	0.4	0.31
WUG_124	1525	0.4	0.48
WUG_121[2]	1550	n/app	0.34

[1] Defined as $-\ln(l_f/l_0)$, where for l_f and l_0 sample length after and before the experiment, respectively, are taken. Includes compaction of the fine-grained olivine matrix.
[2] Experiment aborted upon reaching experimental pressure and temperature conditions, but before starting advancing the deformation piston.

Olivine powder was also synthesized from inclusion-free olivine fragments. These fragments were crushed with an agate mortar and pestle and subsequently ground in a Syalon™ ball mill for several hours in water, until the maximum particle size of the powder was <10 μm. The olivine and orthopyroxene were packed in a nickel capsule in a 60:40 volume ratio. Simultaneously, olivine powder was sequentially added to fill the void space between the clasts. Porosity of the experimental charge prior to experiments is estimated to be ~15%.

Samples were deformed in a Griggs apparatus using a solid-medium assembly with a crushable MgO inner pressure medium and pyrophyllite outer pressure medium. A 2 mm thick disk of barium carbonate was inserted above the experimental charge to reduce deformation during the initial stages of compression and heating. The assembly was stored in a vacuum oven at 363 K for a minimum of 14 hours prior to experiments to remove any water adsorbed on mineral surfaces during synthesis. Experiments were initiated by raising confining pressure to 0.5 GPa. Pressure and temperature were then raised simultaneously to 1 GPa and 1173 K. Finally, temperature was increased to the target temperature for the experiment, while pressure was maintained (Table 1). The temperature was monitored by a Pt/13%Rh thermocouple located at the middle of the sample. Once experimental conditions were attained, the sample was annealed for two to five hours to allow the olivine powder to compact and sinter. Constant strain-rate deformation was imposed by advancing a piston at constant speed. Samples were deformed until the desired axial strain was achieved. Experiments were quenched and thin-sections cut parallel to the shortening axis.

Bulk natural strain (ε_b) for each experiment (Eq. (1)) was calculated from the initial (l_0) and final (l_f) sample length.

$$\varepsilon_b = -\ln\left(\frac{l_f}{l_0}\right) \tag{1}$$

For each pair of adjacent and unlike clasts, the strain of each clast was calculated individually (ε_c). Most clasts are ellipsoidal in shape after deformation, with a minor axis that is subparallel to the macroscopic sample shortening. Dimensions of clasts were determined by the software package ImageJ 1.46r (http://rsbweb.nih.gov/ij/) using digitized cross-polarized photomicrographs. The strain of each clast was calculated from the length

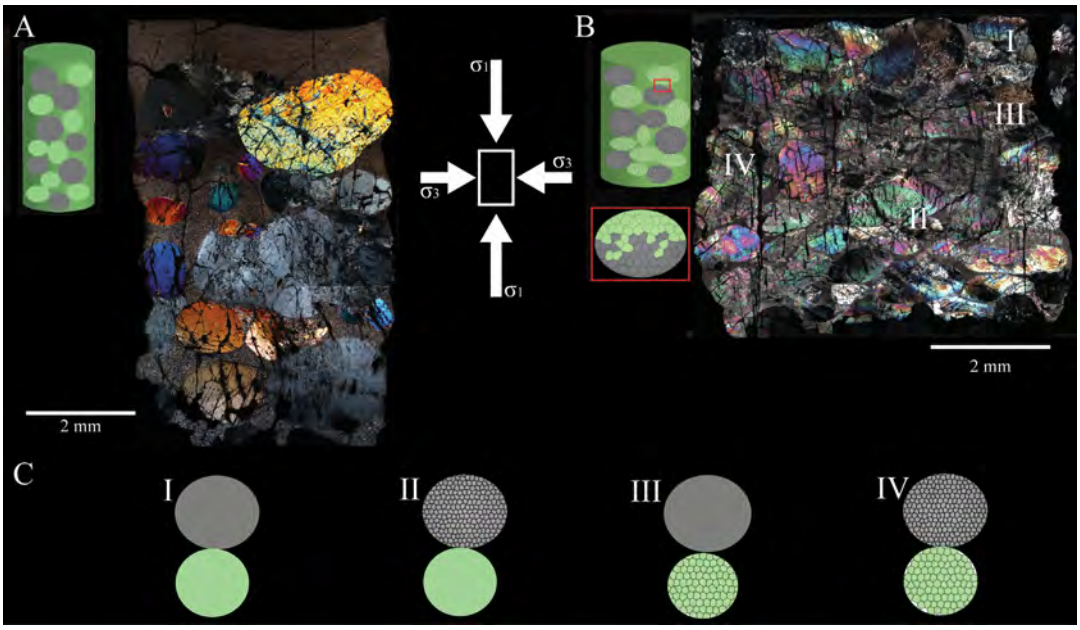

Fig. 1. Photomicrographs of thin-sections from two experiments, with inset cartoons schematically illustrating the associated microstructures. The initial length of both experiments was 12.3 mm. Shortening direction is vertical. (A) Sample (WUG_121) quenched during the annealing stage. Clasts were largely unaffected by the initial stage of compaction and annealing. (B) Compacted and highly deformed sample (WUG_113) showing deformed and recrystallized clasts. (C) Schematic illustrations of the four types of olivine/orthopyroxene interfaces: I) relict (unrecrystallized) olivine and orthopyroxene, II) relict olivine and recrystallized orthopyroxene, III) recrystallized olivine and relict orthopyroxene, and IV) recrystallized olivine and orthopyroxene. Examples of each interface type are labeled in (B).

of the minor axis. The length of the pre-deformation minor axis of the clast was calculated assuming constant volume deformation of an ellipsoidal shape with an aspect ratio of 1.25.

Detailed microstructural mapping at selected domain interface boundaries was conducted by electron backscatter diffraction (EBSD). Point-by-point determination of the orientation of crystals, expressed in Euler angles maps, allows for the identification of grain and subgrain boundaries. Additional information on the quality of the EBSD pattern (the band contrast) provides a convenient tool for distinguishing crystalline grains from grain boundaries. As each mineral has a unique electron backscatter diffraction pattern, EBSD also allows for phase identification.

EBSD analyses were performed on a JEOL 7001LVF FE-SEM (Field Emission-Scanning Electron Microscope) operated at low vacuum conditions (10 Pa), at an acceleration voltage of 20 kV and a beam current of 15–20 nA. Typical step-sizes for these analyses were 0.25–1.00 μm. HKL technology's Channel 5 software suite was used to acquire and process EBSD data.

Grain size analyses were performed on maps of band-contrast data that were collected along with the orientation data, and which clearly reveal grain boundaries. The recrystallized grain-sizes of olivine and orthopyroxene were measured using the mean-intercept method, with a stereological correction factor of 1.5. Using the olivine recrystallized grain-size piezometer of Van der Wal et al. (1993) the differential stress at continuous olivine–orthopyroxene domain interfaces was calculated. Van der Wal et al. (1993) uses the same mean-intercept method for determining grain-size, although they make different assumptions about grain shape, which yields a stereological correction factor that is smaller by ∼10%.

3. Results

Experiments yielded deformed samples with axial strain ranging from 0.31 to 0.74 (Table 1). Initial shortening of the capsule is mainly accommodated by the compaction of the fine-grained olivine matrix. Subsequent deformation is accommodated by plastic deformation of the fine-grained olivine matrix and the olivine and orthopyroxene clasts.

Experiments quenched during the annealing stage show that the clasts were largely unaffected by the initial compaction and sintering. Some brittle fracturing was observed, including cracks caused by loading and identified by the infilling of cracks by matrix powder, and unloading cracks that crosscut multiple clasts and dense matrix. Areas unaffected by these cracks are used in the subsequent interpretation of the microstructural data. Beyond this initial stage of compaction and sintering, deformation within the clasts is identified by a progression of microstructural changes.

Strain in these samples is heterogeneous and the amount of strain accumulated by each clast varies within a single experiment, regardless of the deformation conditions. Clasts frequently exhibit an internal strain gradient and those that are in contact with one or more neighbors display evidence for more deformation in comparison to clasts that are surrounded by fine-grained matrix. Concentrations of strain in these cases are likely caused by the mutual impingement of clasts, which are initially stronger than the fine-grained matrix by one to two orders of magnitude (Hirth and Kohlstedt, 2003).

Boundaries between olivine and orthopyroxene clasts are described by four generic types of interfaces (see Fig. 1C for interface descriptions). 89 interfaces were identified and characterized. To investigate phase mixing, we focus on type IV interfaces, in which both olivine and orthopyroxene are recrystallized. Type IV interfaces are observed infrequently, representing ∼19% ($n = 17$) of the interfaces identified. These are distributed over seven samples from experiments at 1400 K, 1500 K and 1525 K (Table 2). Within the subset of type IV interfaces, natural strain of the olivine clasts varies from 0.12 to 1.05. The strain of orthopyroxene clasts is often higher than for olivine clasts and varies from 0.09 to 2.36 (Table 2).

The Schmid factor for olivine and orthopyroxene clasts was determined for the [100](010) and [001](100) slip systems, respectively, which are expected to be the dominant slip-systems at these experimental deformation conditions (Bai et al., 1991; Jung and Karato, 2001; Ross and Nielsen, 1978). The Schmid factor for olivine clasts ranges from 0.01 to 0.47 and from 0.02 to 0.39 for

Table 2
Type IV interfaces. Strain (ε_c), recrystallized grain size and Schmid factor for the olivine (Ol) and orthopyroxene (Opx) clasts at either side of the interface. Data from clasts with multiple interfaces are repeated for each interface. Values in parentheses are one-standard-deviation error values. Grain size is only listed for interfaces at a high angle to the shortening axis.

Experiment	Interface ID	Ol ε_c (%)[1]	Ol grain size (μm)	Ol Schmid factor [100](010)	Opx ε_c (%)[1]	Opx grain size (μm)	Opx Schmid factor [001](100)	Phase mixing
WUG_64	E2	0.18	2.6	0.03 (0.01)	0.70		0.03 (0.01)	No
WUG_18	A	0.64	20.2	0.41 (0.01)	NA	10.0		Yes
WUG_76	A1	0.13		0.05 (0.02)	1.00		0.02 (0.01)	No
WUG_113	A1	0.34		0.25 (0.02)	2.36		0.24 (0.02)	No
	D	0.52		0.29 (0.01)	1.08		0.07 (0.01)	No
	J	0.77		0.47 (0.03)	2.26		0.09 (0.04)	No
	L	1.05		0.25 (0.02)	2.26		0.09 (0.04)	No
WUG_115	A	0.35		0.05 (0.04)	1.74	3.0	0.21 (0.03)	Yes
	B	0.21	3.8	0.05 (0.03)	0.32	3.8	0.19 (0.02)	No
	D	0.18		0.03 (0.02)	0.46		0.25 (0.05)	No
WUG_119	G	0.20		0.01 (0.01)	0.27	4.6	0.31 (0.02)	Yes
	H	0.13		0.23 (0.01)	0.54	3.8	0.05 (0.02)	No
WUG_124	A	0.33		0.06 (0.02)	0.06		0.39 (0.01)	No
	B	0.12		0.01 (0.01)	0.83		0.29 (0.07)	Yes
	C	0.64	16.2	0.23 (0.05)	0.83	9.8	0.29 (0.07)	Yes
	D	0.50		0.38 (0.02)	0.46		0.04 (0.02)	Yes
	H	0.28		0.28 (0.04)	0.15		0.09 (0.03)	No

[1] Error is 0.10 for all measurements.

orthopyroxene (Table 2), where larger values (the maximum possible value is 0.5) represent grains that are favorably oriented for shear. There is only a weak relationship between the Schmid factor and the strain observed in individual clasts.

Microstructural features of deformation are difficult to resolve using light microscopy at the thin-section scale. Some undulose extinction, occurring at the length scale of 10–20 μm and increasing in intensity towards clast–clast contacts, is observed. At high magnification, patches of small grains can be identified. Higher resolution microstructural data was obtained using EBSD, focusing on interfaces that were identified using light microscopy.

Euler angle maps illustrate the replacement of relict clast material by fine grains or neoblasts (Fig. 2A, C). Relict material displays evidence for lattice distortion in the form of low-angle interfaces that are interpreted as subgrain boundaries. The spacing of the subgrain boundaries is comparable with the grain-size of the neoblasts. Between subgrain boundaries, there is little internal distortion of the crystal lattice. The neoblasts are euhedral in shape and do not exhibit any internal distortion (Fig. 2A, C). Grain boundaries are typically straight or gently curved. Olivine, in particular, often exhibits near equilibrium 120° triple junctions. The crystallographic preferred orientation (CPO) of the neoblasts shows point maxima that overlap with the orientation of the associated relict grains (Fig. 3B, D). The microstructure at type IV interfaces is also characterized by a grain size contrast between recrystallized olivine and orthopyroxene. Recrystallized orthopyroxene grains are typically smaller than the neighboring olivine grains (Table 2). Recrystallized olivine ranges in size from 2.6 to 20.2 μm, whereas the grain size of recrystallized orthopyroxene varies between 3.0 and 10.0 μm.

On high-resolution EBSD maps of type IV interfaces, phase boundaries (i.e. grain boundaries between adjacent olivine and orthopyroxene neoblasts) often appear serrated (Fig. 3). In most cases, this serration occurs along triple junctions where both olivine and orthopyroxene are present (solid white arrows in Fig. 3A). The wavelength of these serrations is roughly the recrystallized grain size of the orthopyroxene (the smaller of the two recrystallized phases). The amplitude of the serration is commonly 1–2 μm, but in some cases may be comparable to the recrystallized grain size. In some cases, grains that fill the serrated notches may be separated from the rest of the recrystallized domain by high angle grain boundaries (dotted white arrows, Fig. 3A–B). At six of the type IV interfaces, we observe mixing of olivine and orthopyroxene along the boundary (Table 2, Fig. 3B). In these examples, grains of one phase are completely surrounded by grains of the other phase. The grain size of these enclaves is comparable to the surrounding grains and in the case of olivine is smaller than the grain-size of the unmixed olivine grains. The distance of the enclaves away from the mono-mineralic domains does not exceed ~3 recrystallized grain-lengths. Notably, extensive phase mixing is not observed. Over the narrow range of conditions that were experimentally achieved in this study, we observe no clear relationship between the degree of phase mixing, temperature, or strain.

4. Discussion

4.1. Grain size reduction and orthopyroxene piezometer

In our experiments, large clasts of olivine and orthopyroxene are progressively replaced by fine-grained material, which we interpret to be the product of dynamic recrystallization. Relict clasts occasionally contain subgrain boundaries (Fig. 2A, C), suggesting that much of the recrystallization is the product of sub-grain rotation recrystallization (e.g. Hirth and Tullis, 1992; Platt and Behr, 2011; Shimizu, 2008; Stipp et al., 2002). This interpretation is consistent with the observation that the neoblasts have an orientation inherited from the host clast (Fig. 2B, D) (Karato, 1988). The ratio of the grain-size before and after recrystallization (i.e. from mm-sized clasts to μm-sized neoblasts) is 10^2–10^3, which is comparable with observations from mylonites and ultramylonites and their host rocks in natural shear zones (e.g. Linckens et al., 2011; Précigout et al., 2007; Vissers et al., 1995; Warren and Hirth, 2006).

The grain size of unmixed, recrystallized orthopyroxene is generally smaller than the grain size of recrystallized olivine (Table 2, Fig. 2A, C). This comparison is most evident at type IV interfaces, where both phases are recrystallized but largely unmixed. When these type IV interfaces are at a high angle to the axis of shortening, we assume that clasts on both sides of the boundary experience the same stress. We estimate the stress at the interface using

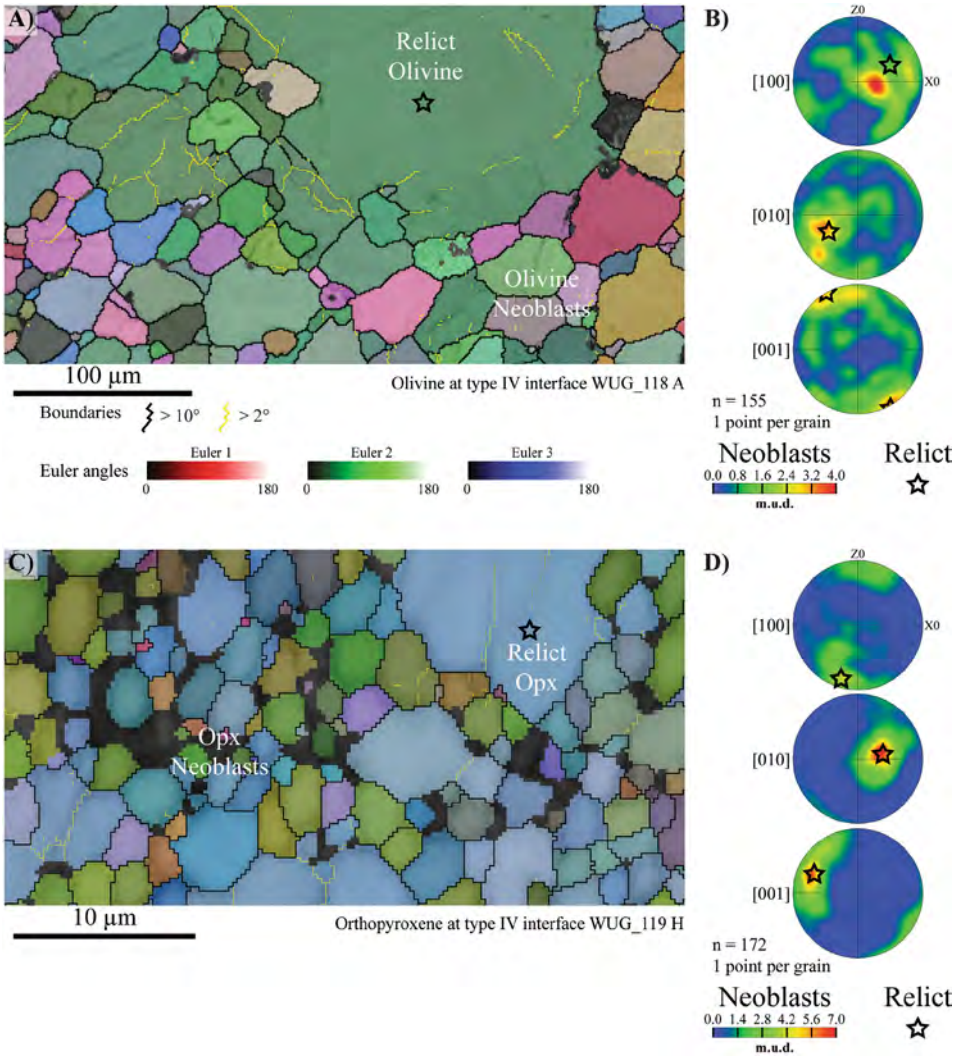

Fig. 2. EBSD data of relict grains and neoblasts for olivine (A–B) and orthopyroxene (C–D). Crystal orientation maps (A, C) were constructed by automatic indexing using HKL's Channel 5.0 fast acquisition software. Misindexed points due to pseudosymmetry in olivine were removed and zero-solution points were artificially indexed by extrapolating the crystal orientation of five or more of its nearest neighbors. Misorientations between neighboring points greater than 2° and greater than 10° are represented by a thin yellow and thick black line, respectively. Step-sizes in (A) and (C) are 0.75 and 0.25 µm, respectively. (B–D) Upper-hemisphere equal-area-projection pole figures for orthorhombic olivine (B) and orthopyroxene (D). The crystal orientation of the associated relict grain is represented by a star. Colors show the density of crystal orientation data for the neoblasts, applying a one-point-per-grain analysis, with multiples of uniform distribution (m.u.d.) ranging from 0.0 to 4.0 (olivine) or 7.0 (orthopyroxene). (For interpretation of the references to color in this figure legend, the reader is referred to the web version of this article.)

the olivine grain-size piezometer of Van der Wal et al. (1993). This piezometer yields flow stresses for type IV interfaces of 100 to 500 MPa (Fig. 4), the range of which is consistent with the heterogeneous nature of the experimental sample. Combining these data with additional data from recrystallized but unmixed grains from sheared lherzolite xenoliths (Boullier pers. comm., 2013; Jin, 1995; Skemer and Karato, 2008), we derive an empirical recrystallized grain-size piezometer for orthopyroxene (Fig. 4). The best-fit line through the data is a power-law relationship:

$$\sigma_{diff} = 2939^{+1673/-1066} d^{-1.308\pm0.01} \quad (2)$$

where σ_{diff} is differential stress in MPa, and d is grain size in µm. Based on these data the contrast in recrystallized grain size between olivine and orthopyroxene in highly sheared rocks in nature (shear stresses of 10–30 MPa) is predicted to be ~5–10. This contrast in recrystallized grain size is interpreted to be a consequence of the slow grain-growth kinetics in orthopyroxene in comparison to olivine (Skemer and Karato, 2007, 2008).

4.2. Deformation mechanisms

To further evaluate deformation mechanisms operative in our samples, an olivine deformation mechanism map was constructed using the empirical flow laws by Hansen et al. (2011) and Hirth and Kohlstedt (2003) (Fig. 5). The relict clasts plot in the field for dislocation creep, whereas the recrystallized grains, constrained by the olivine piezometers by Van der Wal et al. (1993) and Karato et al. (1980) plot in the field for disGBS (Hansen et al., 2011; Hirth and Kohlstedt, 2003). This indicates that relict clasts and recrystallized grains deformed by different mechanisms. The existence of subgrains, confirms that the relict clasts deformed by dislocation creep. Microstructural comparison with peridotite experimentally deformed in the semi-brittle field (Druiventak et al., 2011) corroborates the assertion that deformation microstructures described here are the result of plastic deformation. No flow laws exist for orthopyroxene in grain-size sensitive regimes (Lawlis, 1998), so we can only speculate by analogy that diffusion creep or disGBS may also be the predominant deformation mechanism in recrystallized orthopyroxene at these conditions (Skemer and Karato, 2008).

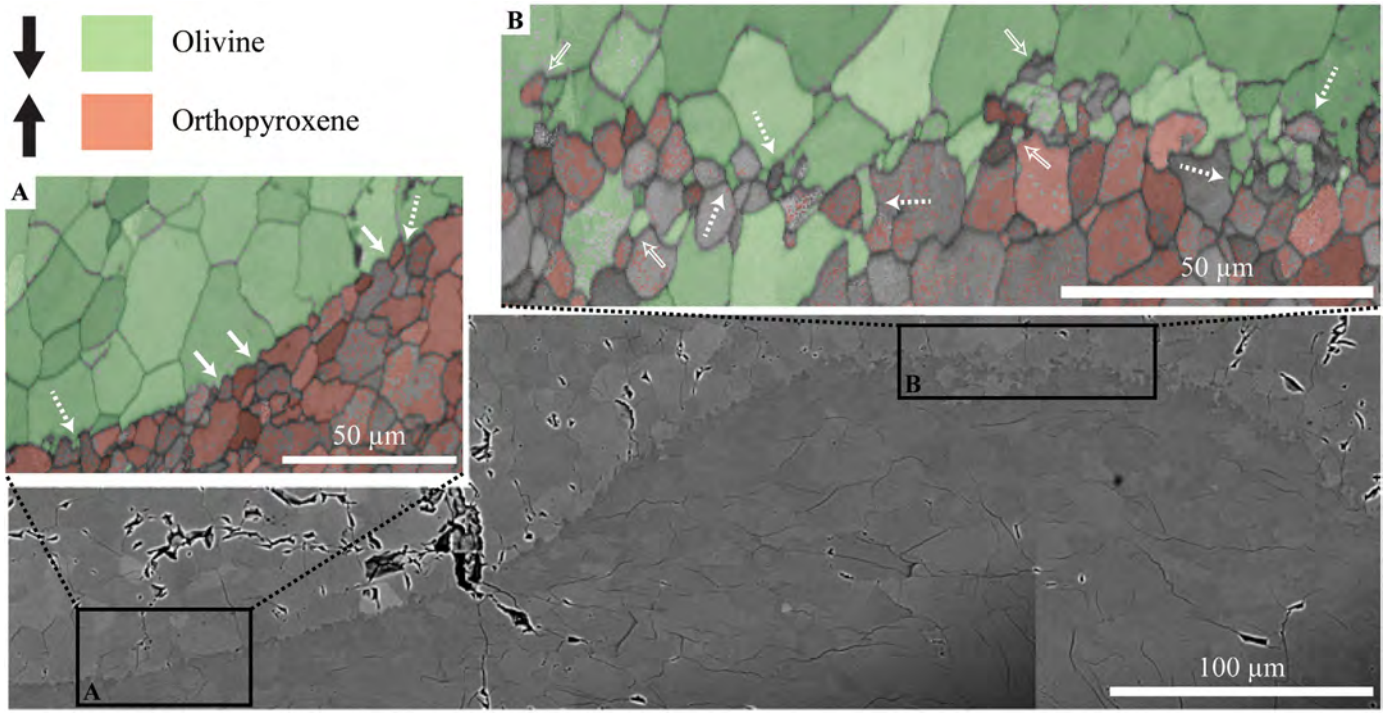

Fig. 3. Back-scatter electron (BSE) image of interface WUG_18 A (bottom) and EBSD-derived band-contrast and phase maps showing the serrated phase boundary at type IV interfaces (A) and a minor amount of intermixed olivine and orthopyroxene (B). Solid arrows point to several locations where the serrated domain occurs at the location of a three-grain triple junction. Dotted arrows highlight examples of serrated domains that are separated from the rest of the recrystallized grains by a high angle boundary. Mixing is observed in some locations, with individual enclaves of one phase completely surrounded by the other phase (open white arrows). However this mixing is limited to a few grain lengths scales (a few tens of microns) from the original interface boundary.

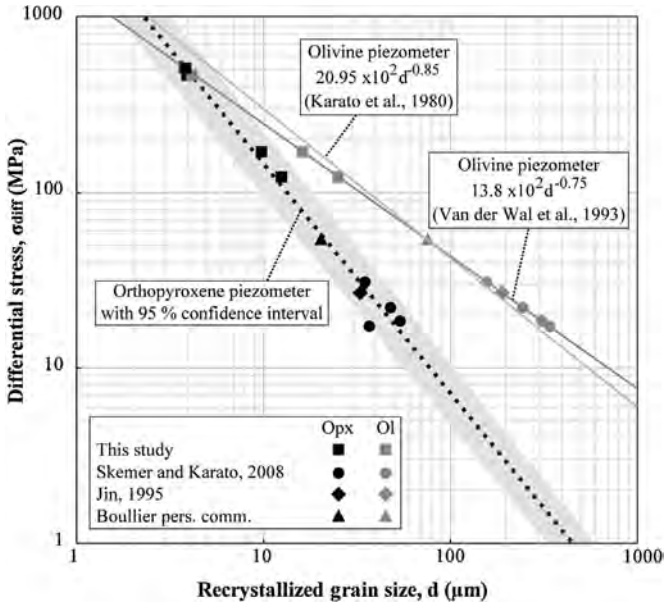

Fig. 4. Plot of differential stress against grain-size for our experiments, as well as some recrystallized unmixed, lherzolite xenoliths from Skemer and Karato (2008), Jin (1995), and Boullier and Gueguen (1975). By definition, olivine data plot along the piezometer of Van der Wal et al. (1993). Corresponding orthopyroxene grains are generally smaller, particularly at low stresses. A best-fit line through the orthopyroxene data defines a new piezometer, which may be used to infer flow stresses in naturally and experimentally deformed orthopyroxene-rich rocks.

4.3. Phase mixing

Grain- or phase-boundary sliding is often invoked as a mechanism for high temperature solid-state phase mixing (Farla et al., 2013; Hiraga et al., 2010, 2013; Précigout et al., 2007; Warren and Hirth, 2006). Where mixing is inferred to occur by grain-switching events, the degree of mixing is predicted to depend on the magnitude of strain imposed (e.g. Ashby and Verall, 1973). However, several other processes may also lead to phase mixing in highly sheared rocks. Dijkstra et al. (2002) hypothesized that silica-undersaturated melt may preferentially corrode orthopyroxene clasts, replacing them with olivine, producing a fine-grained, well-mixed microstructure. While channelized melt is often associated with mantle shear zones (Kelemen and Dick, 1995; Higgie and Tommasi, 2012), melt corrosion is not likely to be important in our experiments, which were conducted at sub-solidus conditions. Other authors have postulated that a phase instability followed by heterogeneous nucleation may introduce phase mixing (Kilian et al., 2011; Kruse and Stünitz, 1999; Newman et al., 1999). However, the olivine–orthopyroxene system is in equilibrium at the experimental pressure and temperatures investigated, and no reactions are expected or reaction products observed. Cataclasis, involving frictional sliding of clasts, may generate phase mixing as well (Goodwin and White, 2003; Jaroslow et al., 1996) but is not relevant at the pressure and temperature conditions of our study.

Of the 17 type IV interfaces identified in this study, the majority do not exhibit any signs of phase mixing. Along un-mixed interfaces, we observe serrations in the phase boundary, which are spatially associated with the presence of triple junctions (Fig. 3A). Our interpretation of this observation is that the margins between recrystallized olivine and orthopyroxene domains are modified by surface tension driven phase boundary migration. During dynamic recrystallization along type IV boundaries, T-shaped triple junctions will form when two recrystallized grains of one phase form adjacent to one grain of a second phase, along a straight phase boundary. As the surface energies of olivine and pyroxene are similar, this grain boundary configuration is energetically unstable (Bulau et al., 1979; Cooper and Kohlstedt, 1982). Phase boundary migration (cf. Sundberg and Cooper, 2008) will allow the mi-

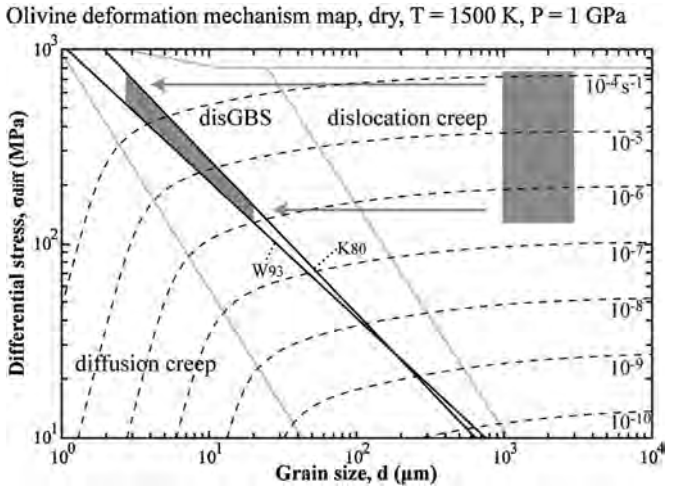

Fig. 5. Deformation mechanism map for olivine, calculated using flow laws from Hansen et al. (2011), and Hirth and Kohlstedt (2003). Shaded boxes depict the experimental conditions before (right) and after (left) recrystallization (arrows). Grain-size refinement during dynamic recrystallization allows the dominant deformation mechanism the change from dislocation creep to dislocation-accommodated grain boundary sliding (disGBS). Dashed lines are contours of constant strain rate curves. The olivine grain-size piezometers (black lines) by Karato et al. (1980) (K_{80}) and Van der Wal et al. (1993) (W_{93}) were used to constrain stress estimates following dynamic recrystallization.

crostructure to equilibrate so grain boundaries meet at more favorable 120° angles. This microstructural equilibration will produce a serrated margin along type IV interfaces with a wavelength approximately equal to the grain-size, and may serve as nucleation points for subsequent phase mixing.

Along six of the type IV interfaces we observe some mixing of olivine and orthopyroxene. In these rare cases, phase mixing is identified as enclaves of olivine surrounded by orthopyroxene, although in some cases we also observe enclaves of orthopyroxene surrounded by olivine (Fig. 3B). However, in contrast to most peridotite mylonites, the degree of mixing is minor, occurring over just a few recrystallized grain length-scales from the original interface boundary. We speculate that this may represent a precursor to more extensive mixing, which would require more recrystallization, phase boundary migration, and grain-switching events, and therefore larger strains.

4.4. Implications for shear localization in Earth

For grain-size reduction and subsequent disGBS to be a viable strain weakening mechanism in polymineralic rocks, two serial microphysical processes are required: (1) grain size must be reduced to switch the dominant deformation mechanism from grain-size insensitive dislocation creep to grain-size sensitive diffusion creep or disGBS (Hansen et al., 2011; Hirth and Kohlstedt, 2003; Rutter and Brodie, 1988; Walker et al., 1990), and (2) grains of different phases must exchange positions to prevent grain growth (Farla et al., 2013; Herwegh et al., 2011; Linckens et al., 2011; Précigout et al., 2007). For this shear weakening mechanism to play an important role in the initiation of localization, these microstructural changes must be generated by small perturbations in a strain field (Skemer et al., 2013).

Our experiments clearly demonstrate that phase mixing between olivine and orthopyroxene is possible under solid-state conditions, but inefficient at moderate temperature and strain, with mixing occurring infrequently and over short length scales. If disGBS is the primary mechanism for phase mixing in the lithospheric mantle, some combination of lower temperature, which enhances disGBS (Hansen et al., 2011), and larger strains are likely needed to reproduce geological observations. Recent large-strain shear experiments on fine-grained pre-mixed olivine–orthopyroxene support the hypothesis that phase mixing is better developed in rocks that are more highly deformed (Farla et al., 2013). However, this may not always be the case, as phase coalescence has also been observed in nano-crystalline olivine–pyroxene aggregates deformed to large strains (Hiraga et al., 2010, 2013). We speculate that phase mixing and phase coalescence may both occur over various mineral domain length scales but our present results cannot reconcile these conflicting observations.

If large strains are required to generate well-mixed steady-state mylonitic microstructure, then strain weakening by grain-size reduction is unlikely to be the primary mechanism for initiating shear localization in Earth's mantle. Other mechanisms that require smaller strain perturbations, for example, feedbacks between the formation of channelized melt and deformation (Aharonov et al., 1995; Stevenson, 1989) or localized hydrolytic weakening (Skemer et al., 2013) would be required to initiate shear localization at high temperatures. The effects of these initial strain perturbations may be amplified by additional microphysical processes such as viscous anisotropy (Hansen et al., 2012; Skemer et al., 2013; Vauchez et al., 2012) or viscous shear heating (Kelemen and Hirth, 2007; Yuen et al., 1978), with long-term shear zone weakness preserved by grain size reduction and phase mixing as described here.

5. Conclusions

There are a number of plausible models for shear localization in Earth and several distinct microphysical processes contribute to the initiation and long-term evolution of a shear zone (Skemer et al., 2013; Vauchez et al., 2012). Grain-size reduction, phase mixing, and a transition to grain-size sensitive creep, is an appealing explanation for strain weakening, as it explains many rheological and microstructural observations from natural shear zones (Linckens et al., 2011; Rutter and Brodie, 1988; Warren and Hirth, 2006). Our deformation experiments reproduce the dynamic recrystallization and subsequent deformation by disGBS inferred to occur in many mantle shear zones. Some mixing is observed along recrystallized phase boundaries, demonstrating that phase mixing is possible in the absence of metamorphic reactions. However, the degree of phase mixing is small in comparison to observations from natural shear zones, with enclaves of mixed grains extending no more than a few recrystallized grain length-scales from the interface boundary. At the moderate strains accessible in these experiments, steady-state microstructures including nearly complete recrystallization and well-developed phase mixing, are not achieved. We conclude that the processes of dynamic recrystallization, phase boundary migration and disGBS deformation may play a critical role in the preservation of weak shear zones over geologic time scales, but do not provide an adequate mechanism for initiating localized deformation in the mantle lithosphere.

Acknowledgements

A.-M. Boullier is thanked for providing grain-size information for the samples described in Boullier and Gueguen (1975). Reviews by K. Michibayashi, V. Toy and E. Mariani, and comments by editor Y. Ricard led to insights that improved this manuscript substantially. This study was supported by NSF EAR-0911289 (to PS) and a grant from the McDonnell Center for Space Studies, Washington University in St. Louis (to RHCB).

References

Aharonov, E., Whitehead, J.A., Kelemen, P.B., Spiegelman, M., 1995. Channeling instability of upwelling melt in the mantle. J. Geophys. Res. 100, 20433–20450. http://dx.doi.org/10.1029/95JB01307.

Ashby, M.F., Verrall, R.A., 1973. Diffusion-accommodated flow and superplasticity. Acta Metall. 21 (2), 149–163. http://dx.doi.org/10.1016/0001-6160(73)90057-6.

Austin, N.J., Evans, B., 2007. Paleowattmeters: A scaling relation for dynamically recrystallized grain size. Geology 35, 343–346. http://dx.doi.org/10.1130/G23244A.1.

Bai, Q., Mackwell, S.J., Kohlstedt, D.L., 1991. High-temperature creep of olivine single crystals 1. Mechanical results for buffered samples. J. Geophys. Res. 96 (B2), 2441–2463. http://dx.doi.org/10.1029/90JB01723.

Bercovici, D., 2003. The generation of plate tectonics from mantle convection. Earth Planet. Sci. Lett. 205, 107–121. http://dx.doi.org/10.1016/S0012-821X(02)01009-9.

Bercovici, D., Ricard, Y., 2012. Mechanisms for the generation of plate tectonics by two-phase grain-damage and pinning. Phys. Earth Planet. Inter. 202–203, 27–55. http://dx.doi.org/10.1016/j.pepi.2012.05.003.

Bercovici, D., Ricard, Y., 2013. Generation of plate tectonics with two-phase grain-damage and pinning: Source-sink model and toroidal flow. Earth Planet. Sci. Lett. 365, 275–288. http://dx.doi.org/10.1016/j.epsl.2013.02.002.

Boullier, A.M., Gueguen, Y., 1975. SP-Mylonites: Origin of some mylonites by superplastic flow. Contrib. Mineral. Petrol. 50, 93–104. http://dx.doi.org/10.1007/BF00373329.

Bulau, J.R., Waff, H.S., Tyburczy, J.A., 1979. Mechanical and thermodynamic constraints on fluid distribution in partial melts. J. Geophys. Res. 84, 6102–6108. http://dx.doi.org/10.1029/JB084iB11p06102.

Bürgmann, R., Dresen, G., 2008. Rheology of the lower crust and upper mantle: Evidence from rock mechanics, geodesy, and field observations. Annu. Rev. Earth Planet. Sci. 36, 531–567. http://dx.doi.org/10.1146/annurev.earth.36.031207.124326.

Carter, N.L., Tsenn, M.C., 1987. Flow properties of continental lithosphere. Tectonophysics 136, 27–63. http://dx.doi.org/10.1016/0040-1951(87)90333-7.

Cooper, R.F., Kohlstedt, D.L., 1982. Interfacial energies in the olivine–basalt system. In: Akimoto, S., Manghnani, M.H. (Eds.), High Pressure Research in Geophysics. Center for Academic Publications, Tokyo, Japan, pp. 217–228.

De Bresser, J.H.P., Peach, C.J., Reijs, J.P.J., Spiers, C.J., 1998. On dynamic recrystallization during solid state flow: Effects of stress and temperature. Geophys. Res. Lett. 25, 3457–3460. http://dx.doi.org/10.1029/98GL02690.

Dijkstra, A.H., Drury, M.R., Vissers, R.L.M., Newman, J., 2002. On the role of melt-rock reaction in mantle shear zone formation in the Othris Peridotite Massif (Greece). J. Struct. Geol. 24, 1431–1450. http://dx.doi.org/10.1016/S0191-8141(01)00142-0.

Druiventak, A., Trepmann, C.A., Renner, J., Hanke, K., 2011. Low-temperature plasticity of olivine during high stress deformation of peridotite at lithospheric conditions — An experimental study. Earth Planet. Sci. Lett. 311, 199–211. http://dx.doi.org/10.1016/j.epsl.2011.09.022.

Drury, M.R., Vissers, R.L.M., Van der Wal, D., Hoogerduijn Strating, E.H., 1991. Shear localisation in upper mantle peridotites. Pure Appl. Geophys. 137, 439–460. http://dx.doi.org/10.1007/BF00879044.

Evans, B., Renner, J., Hirth, G., 2001. A few remarks on the kinetics of static grain growth in rocks. Int. J. Earth Sci. 90, 88–103. http://dx.doi.org/10.1007/s005310000150.

Farla, R.J.M., Karato, S., Cai, Z., 2013. Role of orthopyroxene in rheological weakening of the lithosphere via dynamic recrystallization. Proc. Natl. Acad. Sci. USA 110, 16355–16360. http://dx.doi.org/10.1073/pnas.1218335110.

Furusho, M., Kanagawa, K., 1999. Transformation-induced strain localization in a lherzolite mylonite from the Hidaka metamorphic belt of central Hokkaido, Japan. Tectonophysics 313, 411–432. http://dx.doi.org/10.1016/S0040-1951(99)00215-2.

Goodwin, L.B., White, J.C., 2003. The impact of transient brittle failure on deformation and metamorphism at middle and lower crustal levels. In: Geological Society of America, Annual Meeting 2003. Abstract #21-11.

Handy, M.R., 1989. Deformation regimes and the rheological evolution of fault zones in the lithosphere: the effects of pressure, temperature, grainsize and time. Tectonophysics 163, 119–152. http://dx.doi.org/10.1016/0040-1951(89)90122-4.

Hansen, L.N., Zimmerman, M.E., Kohlstedt, D.L., 2011. Grain boundary sliding in San Carlos olivine: Flow law parameters and crystallographic-preferred orientation. J. Geophys. Res. 116 (B8). http://dx.doi.org/10.1029/2011JB008220.

Hansen, L.N., Zimmerman, M.E., Kohlstedt, D.L., 2012. Laboratory measurements of the viscous anisotropy of olivine aggregates. Nature 492 (7429), 415–418. http://dx.doi.org/10.1038/nature11671.

Herwegh, M., Linckens, J., Ebert, A., Berger, A., Brodhag, S.H., 2011. The role of second phases for controlling microstructural evolution in polymineralic rocks: A review. J. Struct. Geol. 33, 1728–1750. http://dx.doi.org/10.1016/j.jsg.2011.08.011.

Higgie, K., Tommasi, A., 2012. Feedbacks between deformation and melt distribution in the crust–mantle transition zone of the Oman ophiolite. Earth Planet. Sci. Lett. 359–360, 61–72. http://dx.doi.org/10.1016/j.epsl.2012.10.003.

Hiraga, T., Miyazaki, T., Tasaka, M., Yoshida, H., 2010. Mantle superplasticity and its self-made demise. Nature 468, 1091–1094. http://dx.doi.org/10.1038/nature09685.

Hiraga, T., Miyazaki, T., Yoshida, H., Zimmerman, M.E., 2013. Comparison of microstructures in superplastically deformed synthetic materials and natural mylonites: Mineral aggregation via grain boundary sliding. Geology 41, 959–962. http://dx.doi.org/10.1130/G34407.1.

Hirth, G., Kohlstedt, D.L., 2003. Rheology of the mantle wedge. In: Eiler, J. (Ed.), Inside the Subduction Factory. In: Geophys. Monogr., vol. 138. American Geophysical Union, Washington, DC, pp. 83–105.

Hirth, G., Tullis, J., 1992. Dislocation creep regimes in quartz aggregates. J. Struct. Geol. 14, 145–159. http://dx.doi.org/10.1016/0191-8141(92)90053-Y.

Hitchings, R.S., Paterson, M.S., Bitmead, J., 1989. Effects of iron and magnetite additions in olivine–pyroxene rheology. Phys. Earth Planet. Inter. 55, 277–291. http://dx.doi.org/10.1016/0031-9201(89)90076-9.

Jaroslow, G.E., Hirth, G., Dick, H.J.B., 1996. Abyssal peridotite mylonites: implications for grain-size sensitive flow and strain localization in the oceanic lithosphere. Tectonophysics 256, 17–37. http://dx.doi.org/10.1016/0040-1951(95)00163-8.

Ji, S., Wang, Z., Wirth, R., 2001. Bulk flow strength of forsterite–enstatite composites as a function of forsterite content. Tectonophysics 341, 69–93. http://dx.doi.org/10.1016/S0040-1951(01)00191-3.

Jin, D., 1995. Deformation microstructures of some ultramafic rocks. MSc Thesis. University of Minnesota, Minneapolis, p. 115.

Jin, D., Karato, S., Obata, M., 1998. Mechanisms of shear localization in the continental lithosphere: inference from the deformation microstructures of peridotites from the Ivrea zone, northwestern Italy. J. Struct. Geol. 20, 195–209. http://dx.doi.org/10.1016/S0191-8141(97)00059-X.

Jung, H., Karato, S., 2001. Water-induced fabric transitions in olivine. Science 293 (5534), 1460–1463. http://dx.doi.org/10.1126/science.1062235.

Karato, S., 1988. The role of recrystallization in the preferred orientation of olivine. Phys. Earth Planet. Inter. 51, 107–122. http://dx.doi.org/10.1016/0031-9201(88)90029-5.

Karato, S., 1989. Grain growth kinetics in olivine aggregates. Tectonophysics 168 (4), 255–273. http://dx.doi.org/10.1016/0040-1951(89)90221-7.

Karato, S., Toriumi, M., Fujii, T., 1980. Dynamic recrystallization of olivine single crystals during high-temperature creep. Geophys. Res. Lett. 7 (9), 649–652. http://dx.doi.org/10.1029/GL007i009p00649.

Kelemen, P.B., Dick, H.J.B., 1995. Focused melt flow and localized deformation in the upper mantle: Juxtaposition of replacive dunite and ductile shear zones in the Josephine peridotite, SW Oregon. J. Geophys. Res. 100 (B1), 423–438. http://dx.doi.org/10.1029/94JB02063.

Kelemen, P.B., Hirth, G., 2007. A periodic shear-heating mechanism for intermediate-depth earthquakes in the mantle. Nature 446 (7137), 787–790. http://dx.doi.org/10.1038/nature05717.

Kilian, R., Heilbronner, R., Stünitz, H., 2011. Quartz grain size reduction in a granitoid rock and the transition from dislocation to diffusion creep. J. Struct. Geol. 33, 1265–1284. http://dx.doi.org/10.1016/j.jsg.2011.05.004.

Kirby, S.H., 1985. Rock mechanics observations pertinent to the rheology of the continental lithosphere and the localization of strain along shear zones. Tectonophysics 119, 1–27. http://dx.doi.org/10.1016/0040-1951(85)90030-7.

Kruse, R., Stünitz, H., 1999. Deformation mechanisms and phase distribution in mafic high-temperature mylonites from the Jotun Nappe, southern Norway. Tectonophysics 303, 223–249. http://dx.doi.org/10.1016/S0040-1951(98)00255-8.

Lawlis, J.D., 1998. High temperature creep of synthetic olivine–enstatite aggregates. PhD Thesis. Penn State University, State College, p. 132.

Linckens, J., Herwegh, M., Müntener, O., Mercolli, I., 2011. Evolution of a polymineralic mantle shear zone and the role of second phases in the localization of deformation. J. Geophys. Res. 116 (B6). http://dx.doi.org/10.1029/2010JB008119.

McDonnell, R.D., Peach, C.J., van Roermund, H.L.M., Spiers, C.J., 2000. Effect of varying enstatite content on the deformation behavior of fine-grained synthetic peridotite under wet conditions. J. Geophys. Res. 105 (B6), 13535–13553. http://dx.doi.org/10.1029/1999JB900412.

Michibayashi, K., Suzuki, M., Komori, N., 2013. Progressive deformation partitioning and recrystallization of olivine in the lithospheric mantle. Tectonophysics 587, 79–88. http://dx.doi.org/10.1016/j.tecto.2012.07.008.

Newman, J., Lamb, W.M., Drury, M.R., Vissers, R.L.M., 1999. Deformation processes in a peridotite shear zone: reaction-softening by an H_2O-deficient, continuous net transfer reaction. Tectonophysics 303, 193–222. http://dx.doi.org/10.1016/S0040-1951(98)00259-5.

Olgaard, D.L., Evans, B., 1986. Effect of second-phase particles on grain growth in calcite. J. Am. Ceram. Soc. 69 (11), C272–C277.

Platt, J.P., Behr, W.M., 2011. Grainsize evolution in ductile shear zones: Implications for strain localization and the strength of the lithosphere. J. Struct. Geol. 33, 537–550. http://dx.doi.org/10.1016/j.jsg.2011.01.018.

Précigout, J., Gueydan, F., Gapais, D., Garrido, C.J., Essaifi, A., 2007. Strain localisation in the subcontinental mantle — a ductile alternative to the brittle mantle. Tectonophysics 445 (3–4), 318–336. http://dx.doi.org/10.1016/j.tecto.2007.09.002.

Regenauer-Lieb, K., Yuen, D.A., Branlund, J., 2001. The initiation of subduction: Criticality by addition of water?. Science 294, 578–580. http://dx.doi.org/10.1126/science.1063891.

Ross, J.V., Nielsen, K.C., 1978. High-temperature flow of wet polycrystalline enstatite. Tectonophysics 44, 233–261. http://dx.doi.org/10.1016/0040-1951(78)90072-0.

Rozel, A., Ricard, Y., Bercovici, D., 2011. A thermodynamically self-consistent damage equation for grain size evolution during dynamic recrystallization. Geophys. J. Int. 184, 719–728. http://dx.doi.org/10.1111/j.1365-246X.2010.04875.x.

Rutter, E.H., Brodie, K.H., 1988. The role of tectonic grain size reduction in the rheological stratification of the lithosphere. Geologische Rundschau 77, 295–307. http://dx.doi.org/10.1007/BF01848691.

Shimizu, I., 2008. Theories and applicability of grain size piezometers: The role of dynamic recrystallization mechanisms. J. Struct. Geol. 30, 899–917. http://dx.doi.org/10.1016/j.jsg.2008.03.004.

Skemer, P., Karato, S., 2007. Effects of solute segregation on the grain-growth kinetics of orthopyroxene with implications for the deformation of the upper mantle. Phys. Earth Planet. Inter. 164 (3–4), 186–196. http://dx.doi.org/10.1016/j.pepi.2007.06.011.

Skemer, P., Karato, S., 2008. Sheared lherzolite xenoliths revisited. J. Geophys. Res. 113 (B7). http://dx.doi.org/10.1029/2007JB005286.

Skemer, P.A., Warren, J.M., Kelemen, P.B., Hirth, G., 2010. Microstructural and rheological evolution of a mantle shear zone. J. Petrol. 51 (1–2), 43–53. http://dx.doi.org/10.1093/petrology/egp057.

Skemer, P.A., Warren, J.M., Hansen, L.N., Hirth, G., Kelemen, P.B., 2013. The influence of water and LPO on the initiation and evolution of mantle shear zones. Earth Planet. Sci. Lett.. http://dx.doi.org/10.1016/j.epsl.2013.05.034.

Smith, C.S., 1948. Grains, phases, and interfaces: An interpretation of microstructure. Trans. AIME 175, 15–51.

Stevenson, D.J., 1989. Spontaneous small-scale melt segregation in partial melts undergoing deformation. Geophys. Res. Lett. 16 (9), 1067–1070. http://dx.doi.org/10.1029/GL016i009p01067.

Stipp, M., Stünitz, H., Heilbronner, R., Schmid, S.M., 2002. The eastern Tonale fault zone: a 'natural laboratory' for crystal plastic deformation of quartz over a temperature range from 250 to 700 °C. J. Struct. Geol. 24, 1861–1884. http://dx.doi.org/10.1016/S0191-8141(02)00035-4.

Sundberg, M., Cooper, R.F., 2008. Crystallographic preferred orientation produced by diffusional creep of harzburgite: Effects of chemical interactions among phases during plastic flow. J. Geophys. Res. 113 (B12). http://dx.doi.org/10.1029/2008JB005618.

Tommasi, A., Knoll, M., Vauchez, A., Signorelli, J.W., Thoraval, C., Logé, R., 2009. Structural reactivation in plate tectonics controlled by olivine crystal anisotropy. Nat. Geosci. 2 (6), 423–427. http://dx.doi.org/10.1038/ngeo528.

Toy, V.G., Newman, J., Lamb, W., Tikoff, B., 2010. The role of pyroxenites in formation of shear instabilities in the mantle: Evidence from an ultramafic ultramylonite, Twin Sisters Massif, Washington. J. Petrol. 51, 55–80. http://dx.doi.org/10.1093/petrology/egp059.

Van der Wal, D., Chopra, P., Drury, M.R., Fitz Gerald, J., 1993. Relationships between dynamically recrystallized grain size and deformation conditions in experimentally deformed olivine rocks. Geophys. Res. Lett. 20 (14), 1479–1482. http://dx.doi.org/10.1029/93GL01382.

Vauchez, A., Tommasi, A., Mainprice, D., 2012. Faults (shear zones) in the Earth's mantle. Tectonophysics 558–559, 1–27. http://dx.doi.org/10.1016/j.tecto.2012.06.006.

Vissers, R.L.M., Drury, M.R., Hoogerduijn Strating, E.H., Spiers, C.J., van der Wal, D., 1995. Mantle shear zones and their effect on lithosphere strength during continental breakup. Tectonophysics 249, 155–171. http://dx.doi.org/10.1016/0040-1951(95)00033-J.

Walker, A.N., Rutter, E.H., Brodie, K.H., 1990. Experimental study of grain-size sensitive flow of synthetic, hot-pressed calcite rocks. In: Knipe, R.J., Rutter, E.H. (Eds.), Deformation Mechanisms, Rheology and Tectonics. Geological Society, London, United Kingdom, pp. 259–284.

Warren, J.M., Hirth, G., 2006. Grain size sensitive deformation mechanisms in naturally deformed peridotites. Earth Planet. Sci. Lett. 248, 438–450. http://dx.doi.org/10.1016/j.epsl.2006.06.006.

White, S.H., Burrows, S.E., Carreras, J., Shaw, N.D., Humphreys, F.J., 1980. On mylonites in ductile shear zones. J. Struct. Geol. 2 (1–2), 175–187. http://dx.doi.org/10.1016/0191-8141(80)90048-6.

Yuen, D.A., Fleitout, L., Schubert, G., Froidevaux, C., 1978. Shear deformation zones along major transform faults and subducting slabs. Geophys. J. R. Astron. Soc. 54 (1), 93–119. http://dx.doi.org/10.1111/j.1365-246X.1978.tb06758.x.